Discovery of a small molecule having both potent anti-fibrotic and anti-inflammatory capabilities

Han-Soo Kim,[1,2*] Moon Kee Meang[3*], Saesbyeol Kim, [3] Ji Yong Lee,[4] Baik L. Seong[5], Ik-Hwan Kim,[6] and Byung-Soo Youn[3#]

[1]Department of Biomedical Sciences, Catholic Kwandong University College of Medical Convergence, Gangneung-si, Gangwon-do 25601, Republic of Korea; [2]Basic Research Division, Biomedical Institute of Mycological Resource, College of Medicine, Catholic Kwandong University, Gangneung-si, Gangwon-do 25601, Republic of Korea; [3]Osteoneurogen, Inc., Seoul, 08501, Republic of Korea; [4]Research Institute of Hyperbaric Medicine and Science, Yonsei University Wonju College of Medicine, Wonju-si, Gangwon-do 26426, Republic of Korea; [5]Department of Biotechnology, Yonsei University, Seoul 03722, Republic of Korea and [6]Department of Biotechnology, Korea University, Seoul 02841, Republic of Korea

Running title: A novel anti-fibrotic/anti-inflammatory chromone scaffold compound

*These authors contributed equally.

[#]Corresponding author, E-mail address: byung4jc@gmail.com

Abstracts

Background: Pulmonary and hepatic fibrosis are intractable and fatal human disorders. In our previous study, we found that eupatilin, a chromone-scaffold (CS) derivative (CSD), has a strong anti-fibrotic effect on *in vitro* fibrogenesis as well as a murine lung fibrosis model. Through structure-activity relationship studies, ONG41008 was identified as a more potent anti-fibrotic and anti-inflammatory CS-analog.

Methods: A set of cell imaging studies, transcriptomic analyses, and *in vivo* mouse model involving bleomycin-induced lung fibrosis (BLM) or a murine nonalcoholic steatohepatitis (NASH) model were conducted to explore how ONG41008 exhibits both anti-fibrotic and anti-inflammatory capabilities. *In vitro* anti-inflammatory activity of ONG41008 was also investigated in RAW264.7 cells, a mouse monocytic cell line stimulated with LPS.

Findings: ONG41008 dismantled latent transforming growth factor complex (LTC), limiting TGFβ to TGFβ receptor via depolymerization of F-actin. ONG41008 was able to reverse pathogenic myofibroblasts into non-pathogenic cell types confirmed by both cell shape changes and global transcriptomics analyses. Expression of macrophages homing chemokines in mouse hepatic stellate cells (HSCs) was significantly mitigated by ONG41008. Orally administered ONG41008 significantly improved onset of lung fibrosis. Oral administration of ONG41008 significantly diminished nonalcoholic fatly liver disease (NFALD) scores. ONG41008 substantially inhibited the production of proinflammatory cytokines, including TNFα and several important chemokines affecting T cells or macrophages. TNFα was situated at the central nod in the LPS-ONG41008-macrophages interactome. ONG41008 inhibited endocytosis of CD14, a LPS coreceptor

Interpretation: ONG41008 could be a potent drug for a broad range of fibrotic diseases or hyper-inflammatory diseases.

Funding: an Osteoneurogen intramural fund

Key words

Fibrosis, Pathogenic myofibroblasts, Macrophages, Cell reversion, TGFβ

Research in context

Evidence before this study:

We previously showed that eupatilin containing a chromone-scaffold (CS) exclusively found in the plant kingdom effectively prevented *in vitro* fibrogenesis as well as in bleomycin-induced lung fibrosis model. Importantly, cell reversion representing pathogenic myofibroblasts (pMFB) to an intermediate cell type occurred *in vitro*, and restimulation of the intermediate cell type was trans-differentiated by long exposure to TGFβ, strongly suggesting that this kind of flexible cell reversion would exist *in vivo* and shed into light on regenerative capacity in fibrotic diseases. One notable feature associated with eupatilin was able to inhibit epithelial-mesenchymal transition (EMT), which plays a central role in initiation and perpetuation of tissue scarring.

Added value of this study:

Furthering these intriguing therapeutic capabilities, a more effective and stable analog of eupatilin, called ONG41008, was generated and subjected to ameliorating fibrogenesis and inhibiting the various disease activities associated with pMFB. We found that ONG41008 was a potent inhibitor of TGFβ biogenesis such that binding of active TGFβ to TGF receptor (TGFR) was limited, resulting in cessation of TGFR signaling and EMT was completely inhibited, leading to lesser fibrogenesis. Interestingly, ONG41008-treated pMFB underwent generation of a hybrid interactome comprising of a major nuclear reprogramming one and a minor residual fibrogenic interactome, suggesting that ONG41008 is a driver of cell reversion as we saw in the previous study of eupatilin. Macrophages have been well appreciated for liver inflammation and innate immunity. It turned out that ONG41008 was able to block macrophages-chemoattracting proteins called chemokines and directly acted on macrophages, resulting in blocking gene expression of various proinflammatory and inflammatory cytokines.

Implications of all the available evidence:

All data considered, we believe that ONG41008 is a potent anti-fibrotic drug candidate. And its effectiveness seems likely related to inhibition of macrophage activation. Accordingly, ONG41008 could be used for dysfunctional immunometabolism like NASH as well as blocking the macrophages-mediated innate immunity like rheumatoid arthritis.

Introduction

Idiopathy pulmonary fibrosis (IPF) is defined a rare disease belonging to interstitial lung diseases (ILD) [1]. Its mortality and morbidity are becoming significant such that the median survival of patients with IPF is 3~5 years after diagnosis and the majority of patients would succumb to death within 5 year of diagnosis [2]. Nonalcoholic fatly liver disease (NFALD) is becoming pandemic over the world due to over-nutrition. Nonalcoholic steatohepatitis (NASH) is an extreme manifestation of NAFLD associated with multiple-parallel immunometabolic dysfunctions such as steatosis, lobular inflammation or progressive fibrosis [3, 4]. It has been well appreciated that mitigation of liver fibrosis is the limiting step for attenuating NASH [5]. Therefore, development of both potent anti-fibrotic and anti-inflammatory drugs is of paramount importance for dealing with IPF or NASH.

Myofibroblasts (MFB) play a central role in the initiation and perpetuation of fibrosis [6]. While identification of the IPF-initiating cells remains to be discovered HSCs are the major cell types contributing to both liver inflammation and liver fibrosis [7]. Although fibrogenic signature proteins such as Collagens, CTGF (connective tissue growth factor) or Periostin have been well elucidated, full spectrum of fibrogenic proteins have yet to be discovered. Nevertheless, several anti-fibrotic modalities have continually put on clinical studies [8]. Although fibrosis is not defined an immune disorder, inflammatory cells are believed to be responsible for eliciting fibrogenic signaling. Among these cells macrophages including bone-marrow-derived ones or tissue residential macrophages like Kupffer cells in the liver may play important roles in establishing early stage inflammation by producing proinflammatory cytokines such as TNFα or IL-1β and probably indirectly affecting TGFβ [9]. Therefore, controlling these proinflammatory cytokines or TGFβ may lead to an efficient modality for fibrotic diseases.

Flavones are members of the polyphenol family, a group of over 10,000 compounds have been exclusively found in the plant kingdom [10]. In general, these phytochemicals protect plants from radiation damage [11]. Due to their anti-oxidant and anti-inflammatory potentials, flavones have long been used to treat inflammatory diseases such as arthritis and asthma [12]. Chromone, 1,4-benzopyrone-4-one, is a central chemical scaffold hereinafter called chromone-scaffold (CS) constituting flavones and isoflavones [13], and the CS derivatives (CSD) are a diverse family based on branching chemical residues coupled to the core CS framework [14]. We recently reported that eupatilin, a CSD from an *Artemisia* species dramatically inhibited LPS-induced osteoclastogenesis via actin depolymerization [15] and downregulation of multiple genes involved in EMT. Here, we show that a noble synthetic CSD, called ONG41008, was able to reprogram EMT and induce reversion of pathogenic myofibroblasts to an intermediate non-myofibroblasts-like cell type, ameliorating lung fibrosis in mouse BLM [16]. In addition to this, ONG41008 blocked LPS-induced macrophage activation via blocking the endocytosis of CD14, independently of TGFβ. This observation may open a door as a powerful new therapeutic modality for treating IPF as well as liver fibrosis in NASH or autoreactive T cells-mediated hyper-inflammation.

Results

Toxicity and DMPK study on ONG41008

Non-GLP (Good Laboratory Practice) toxicokinetic studies using rats told us that ONG41008 existed in plasma over 12 hr via oral administration, resulting in T_{max} (1 hr) with C_{max} (260.8ng ± 41.4ng) as seen in Supplementary Figure 1A. The AUC_{inf} was 426.5 ng hr/ml. A 14 Days' oral gavage assessment rendered non-toxic (data not shown). The same held true for non-GLP single injection oral PK study using beagle dogs (Supplementary Figure 1B). Mice and rats were subjected to tissue PK studies within 2 hr upon oral administration. As seen in Supplementary Figure 2, ONG41008 was rapidly detected from the plasma, lung, liver or kidney tissues of mice or rats within 30 min.

ONG41008 dismantles latent TGFβ complex (LTC) via depolymerization of F-actin.

When ONGHEPA1 (mouse HSC cels) or DHLF (diseased human lung fibroblasts from IPF patients) were stimulated with TGFβ, expression of *αSMA* (α-smooth muscle actinin) was notable but was then substantially mitigated with the treatment of ONG41008 (Figure 1A for ONGHEPA1 and Supplementary Figure 3 for DHLF). Likewise, other fibrinogenic markers involving C*ollagen1α1*, C*ollagen11α1* or *Periostin* was induced by TGFβ and were knocked down by ONG41008, suggesting that ONG41008 may directly act on pathogenic myofibroblasts (pMFP) both in the lung or liver fibrotic tissues. ONG41008 markedly inhibited phosphorylation of both SMAD2 and SMAD3, suggesting that phosphorylated Smad2 and/or Smad3 may translocate to the nucleus, activating fibrogenesis. Vibrant phosphorylation of ERK with ONG41008 remains to be further discovered (Figure 1B).

In our previous study, we showed that eupatilin effectively depolymerized F-actin. Likewise, we hypothesized that F-actin in actin filaments might be also a molecular target for ONG41008. As shown in Figure 1C, actin filaments were apparent in TGFβ-stimulated cells

and the severed actin fragments were uniformly distributed in the cytoplasm upon ONG41008 treatment in the presence of TGFβ. While a massive actin depolymerization was observed with the treatment of ONG41008 no such depolymerization was seen in ONGHEAPA1 cells stimulated with pirfenidone or nintedanib, suggesting that the latter two anti-IPF drugs have little or no effects on F-actin depolymerization. *In vitro* actin polymerization or depolymerization assay was established and showed that ONG41008 was, indeed, an inhibitor of actin polymerization (Figure 1D) as well as an enhancer of actin depolymerization (Figure 1E). It has well been appreciated that osteoclasts exist as fused states whereby the O-ring made of F-actin surrounds the fused osteoclasts called multinucleated osteoclasts [17]. As shown in Supplementary Figure 4, ONG41008-treated multinucleated osteoclasts tremendously gave rise to actin fragmentation. These studies indicate that ONG41008 may be a bona-fide F-actin depolymerizer.

To further elucidate mode of action (MOA) for ONG41008, we stimulated DHLF with TGFβ plus ONG41008 and stained them with various antibodies recognizing the components of LTC. LTC plays a central role of TGFβ biogenesis [18], releasing active TGFβ, which is then engaged in the TGFRI/TGFRII complex, giving rise to phosphorylation of SMAD2/SMAD3. Among the known components, LTBP1 and LAP1 were tremendously induced and secreted into the extra cellular matrix (ECM) compartments with the treatment of TGFβ, but LTBP4 appears to be either only partially affected or unaffected by ONG41008 (Figure 2A). ONGHEPA1 were also treated with TGFβ in the presence or absence of ONG41008 for 24 hr. It is evident that LTBP1, LAP1 and Integrin α5β3 in the presence of ONG41008 were massively downregulated and appears to be localized in endosome-like compartments and actin stress fibers were substantially disintegrated (Figure 2B).

Generation of ONG41008-mediated fibrogenic interactome and identification of NOX4 as an anti-inflammatory component in lung and liver fibrosis.

In order to identify the ONG41008-mediated fibrosis-inducing genes (FIGS), DHLF were differentially stimulated with TGFβ in the presence or absence of ONG41008 and transcriptomic change was analyzed by RNA-seq. Schematic representation of this selection process is shown in Supplementary Figure 5. We nailed down seventy-seven ONG4108-mediated FIGS with p>0.005 (Figure 3). Many of these have been already known to be fibrogenic genes such as *CTGF* (connective tissue growth factor), *PERIOSTIN*, *LOX* (lysyl oxidase), or *N-cadherin (CDH2)* [19-21]. *Elastin (Eln)* gene expression has been appreciated that ELASTIN is prefibrotic and represents progress of fibrosis. And it is known to be an EMT gene [22, 23]. Clear indication is that *Eln* gene expression was substantially induced with TGFβ and was knocked down with ONG41008 whose IC50 was 194 nM (Supplementary Figure 6A). In line with this, secreted ELN protein from DHLF was significantly inhibited with ONG41008 (Supplementary Figure 6B). *NOX4*, a NADPH oxidase, caught our attention because induction of *NOX4* has been reported for production of pronounced reactive oxygen species (ROS) as well as for elicitation of several important signaling events like inflammasome activation [24]. To scrutinize whether ONG41008 is able to suppress induction of *NOX4*, thereby downregulating ROS production, ONGHEPA1 were stimulated with TGFβ and induction kinetics of *NOX4* along with *Collagen11α1* and *Periostin* were analyzed at transcription levels. As shown in Figure 4A, *NOX4* mRNA was gradually induced by TGFβ and ONG41008 was able to block the induction, suggesting that ONG41008 may be able to inhibit *NOX4* at transcription levels. Production of ROS was also significantly attenuated, which is shown by immunocytochemistry (ICC) (Figure 4B). The same held true for DHLF (Figure 4C). Furthermore, ROS production was markedly reduced via ROS dye staining (Figure 4D).

ONG41008 was able to block the induction of *NOX4, CCL2* and *CCL7* (Figure 4E), suggesting that ONG41008 could modulate migration of macrophages to the liver and inflammation in the liver.

ONG41008 reverses TGFβ-induced transdifferentiation of myofibroblast

During the course of this study, it has occurred to our attention that ONG41008 treatment alone reversed the cell fate of pMFB into an intermediate non-pathogenic cell type. To have a deeper understanding on a potential mechanism of cell reversion, we established a series of continual differentiation experiments by using ONGHEPA1, which could be a unique *in vitro* model, in such a way that morphological changes as well as interactome changes were closely monitored. As shown Figure 5A, transdifferentiation into myofibroblasts was established by stimulating ONGHEPA1 cells with TGFβ for 24 hr after which the resultant myofibroblasts were washed off with buffer and were subjected to TGFβ plus ONG41008 or ONG41008 alone (data not shown) for 48 hr because the combinatorial treatment seemed to be more pertinent to *in vivo* situation. The treated cells were re-plated out and continually were stimulated with TGFβ alone for 72 hr. Upon completion of initial transdifferentiation, stimulation of myofibroblasts with TGFβ plus ONG41008 remarkably transformed myofibroblasts into an intermediate cell type. Moreover, these intermediate cells seemed to be situated in quiescence since no conspicuous cell growth was observed. We extended our question to see if these quiescent cells can be again transdifferentiated to myofibroblasts with the treatment of TGFβ alone. We discovered that transdifferentiation resumed at least 48 hr after TGFβ stimulation, suggesting that this reversion process should be a flexible differentiation program *in vitro*. To determine if this remarkable reversion process has to do with nuclear reprogramming, we extensively analyzed global gene expression changes at each

stimulation condition. As shown in Figure 5B, a hybrid interactomes existed in the reversion process; 1) fibrogenic interactome and 2) reversion interactome. The former involves chemokines, collagens, adhesins or enzymes, and ECM biogenic factors as shown in Supplementary Figure 7. The latter is apparently composed of a minor residual fibrogenic interactome and a major nuclear reprograming one. The residual fibrogenic interactome seems to be linked to the major nuclear programming via linking the Spp1(Secreted Phosphoprotein 1)-Egr1(Early Growth Response 1) axis (the former one) and the MKI67 (marker of proliferation Ki-67)-Birc5 (Baculoviral IAP Repeat Containing 5) in the latter one. ONG41008 may generate intermediate cell types via the hybrid interactome. Taken together, the ONG41008-mediated cell reversion is directly related to nuclear reprogramming possibly including chromatin remodeling.

In vivo therapeutic efficacy of ONG41008 for anti-lung fibrosis

Therapeutic efficacy of ONG41008 for lung fibrosis was analyzed via a mouse therapeutic BLM. A greatest reduction in collagen production was observed at ONG41008 50 or 100mpk, whereas no significant inhibition was noted at ONG41008 10mpk as well as at pirfenidone 100mpk (Figure 6A), suggesting that larger exposure of ONG41008 may be needed to cope with existing lung fibrosis in therapeutic model. While production of hydroxy proline (HP) at 10mpk or 50mpk of ONG41008 only exhibited reduction tendency 100mpk significantly inhibited HP production with a statistical significance (Figure 6B). Pirfenidone did not generate reduction in both collagen and HP with statistical significances. Expression of αSMA were more significantly decreased in the ONG41008-treated mice than control mice. However, dexamethasone did not affect αSMA staining, indicating that anti-inflammation may not be able to mitigate proliferation of myofibroblasts at advanced stages (Figure 6C). In a preventive BML, both ONG41008 10mpk and 25mpk were able to significantly attenuate the

lung fibrosis. ONG41008 100mpk did not reach a statistical significance, currently the reason being unknown whereas the HP production at 100mpk was remarkably reduced (Supplementary Figure 8A). Pirfenidone exhibited a moderate reduction in both cases. Pirfenidone only gave rise to decreasing tendencies in reduction of soluble collagen or HP production (Supplementary Figure 8B). Apparently, ONG41008 at three administration concentrations remarkably reduced collagen deposition shown by Masson-Trichome tissue staining whereas dexamethasone was unable to improve the disease severity (Supplementary Figure 8C). Taken together, ONG41008 could be a good candidate for treating IPF as a monotherapy or as a combination therapy with pirfenidone.

ONG41008 is a potent inhibitor of innate immunity in that it could be a TNFα antagonist in macrophages independently of TGFβ

It has been lately reported that knocking out *TNFα* negatively affects steatosis or NFALD score [25]. Since we only explored a potent anti-inflammatory capability associated with ONG41008 in HSC or DHLF in TGFβ-dependent manner, a natural question would be whether its anti-inflammatory property can be extended to macrophages in response to LPS stimulation in the absence of TGFβ. RAW264.7 cells, a mouse monocytic leukemic cell line resembling macrophages, were stimulated with LPS in the presence or absence of ONG41008. As shown in Figure 8A, expression of proinflammatory cytokines or chemokines including *TNFα*, *CCL2*, *CCL7*, *CXCL2* and *CXCL10* were markedly downregulated by ONG41008. Interestingly, *CHOP* was so markedly reduced that formation of inflammasome could be attenuated [26-28]. However, no statistically significant repression of *IL6* or *IL23* was made (data not shown). TNFα protein levels in the culture supernatants were clearly reduced by ONG41008 (Figure 7B). Varying LPS concentrations (100ng/ml to 10μg/ml) showed that

ONG41008 effectively blocked expression of *TNFα*, suggesting that some membrane proximal events might be responsible for the ONG41008-mediated inhibition of *TNFα* gene expression (Supplementary Figure 9). It strongly indicates that ONG41008 may inhibit formation of a TLR4-LPS binding proteome or signalosome such as CD14, MD-2 or Myd88 [29]. This prompted us to explore intracellular trafficking of these proteins upon LPS stimulation. As shown Figure 8A, LPS induced the internalization of CD14 and Myd88, whereas ONG1008 inhibited LPS-dependent CD14 endocytosis, induced a polarized distribution of endocytic CD14 and significantly attenuated of endocytosis of Myd88. Magnified views on these ICC further clearly revealed that ONG41008 blocked the internalization of CD14 to endocytic compartments (Supplementary Figure 10). On the contrary, MD-2 and NOX4 remained largely unaltered (Supplementary Figure 11). An interactome regulating the LPS-ONG41008 axis in macrophages was established based on an RNA-Seq. To our surprise, TNFα turned out to be the central nod of the interactome, strongly suggesting that ONG41008 may play a central role in antagonizing TNFα transcription (Figure 8B).

Summing up all these observations, we believe that ONG41008 is an endocytosis inhibitor of CD14, remarkably diminishing macrophage activation. It should be stressed here that ONG41008 is intrinsically equipped with both anti-inflammatory and anti-fibrotic capabilities suggesting that its applicability could well suit immunometabolic dysfunctions or controlling innate immunity.

In vivo therapeutic efficacy of ONG41008 for anti-NASH

We supposed that these combined anti-inflammatory and anti-fibrotic capabilities associated with ONG41008 may make ONG41008 an ideal drug for NASH. NASH is characterized by fatty liver, lobular inflammation, hepatocyte ballooning and progressive

fibrosis [4]. Due to these multifaceted clinical features, NASH has become the most-challenging immunometabolic ailment [30]. Blockade of either inflammation or/and fibrosis may be able to only partially ameliorate NASH. We adapted the STAM mouse model in which five to eight weeks STAM mice exhibit the most human resembling NASH [31]. STAM mice were orally administered with vehicle, ONG41008 50mpk or 100mpk, Telmisartan 30mpk (positive control) or Obeticholic acid (OCA) 30mpk as negative control. While ONG41008 50mpk gave rise to a clear sign of improvement of fatty liver as seen, no significant improvement of onset of NASH was noted at ONG41008 100mpk. Inhibitory trends in lobular inflammation and hepatocyte ballooning were seen at ONG41008 50mpk. Telmisartan showed clear improvement in all score parameters (Figure 9A). Partial improvement of lobular inflammation or hepatocyte-ballooning was observed by ONG41008 100mpk but did not reach statistics. Pathologic manifestation was scored; 1) steatosis, 2) lobular inflammation and 3) hepatocyte ballooning as well as hepatic fibrosis. This observation revealed that ONG41008 and telmisartan are therapeutically effective for NASH based on NAFLD scores (Supplementary Figure 12). On the contrary, no significant improvement of NASH was noted and little degree of inhibition of fibrosis was also observed with the treatment of OCA 30mpk (data not shown).

Discussion

CSD have been well appreciated for their anti-inflammation capabilities [32]. We recently found that a few CSD are capable of attenuating *in vitro* fibrogenesis and *in vivo* fibrosis [33]. Slight modification of functional groups linked to CSD severely affected degree of anti-fibrosis, suggesting that medicinal chemistry would be able to improve their therapeutic efficacy. One drawback associated with CSD in terms of *in vivo* use for treating fibrosis is that CSD administered into rodents largely used to undergo glucuronidation. We confirmed that glucuronide form of CSD completely lost the anti-fibrotic capacity *in vitro* (data not shown). Thus, development of the analogs coping with this impairment should be implemented. ONG41008 rendered non-toxic when subjected to non-GLP toxicity. PK profiles using rats or beagle dogs via oral administration were readily detectable. In many senses, ONG41008 could be a therapeutically pertinent drug candidate.

The major MOA seems to be able to dismantle LTC in such a way that ONG41008 limits binding of the active TGFβ to TGFRs; one major manifestation is blocking phosphorylation of SMAD2/SMAD3, resulting in disabling type 2 EMT so called fibrogenesis. However, phosphorylation of ERK was not affected by ONG41008, suggesting that ONG41008 is largely associated with the main signaling of TGFR, i.e. phosphorylation of SMAD2/SMAD3. We demonstrated that ONG41008 was able to reverse cell fate of pMFB, which was transdifferentiated from HSC, into an intermediate non-pathogenic myofibroblast-like cell type. This reversion process did not require TGFβ. Continual stimulation with TGFβ in the absence of ONG41008 over 72 hr enabled the intermediated cell type to be then transdifferentiated into myofibroblasts, suggesting that ONG41008-mediated reversion may be an *in vitro* and/or *in vivo* flexible differentiation program. Consistent with generation of a hybrid interactome, the reversion process seemed be controlled at chromatin levels. In particular, it has been noted that this sort of intermediated cell type is often observed from the

biopsy samples of the liver cirrhosis patients [34]. Our *in vitro* demonstration that two distinct interactomes, fibrogenic interactome and nuclear interactome, coexist in the ONG41008-treated myofibroblasts supports the existence of intermediate cell types in liver fibrotic tissues. Nevertheless, how ONG41008 initiates this reversion process remains to be determined in order to discover a molecular target for a central role by ONG41008.

Crucial role of TNFα associated with liver diseases prompted us to scrutinize effect of ONG41008 on macrophage physiology. Macrophages play a central role in inflammation whose activation has been known to be modulated by ROS [35]. As ONG41008 mitigated *NOX4* gene expression in DHLF as well as in ONGHEPA1 (HSC) cells, how ONG41008 regulates *NOX4* gene expression in ONGHEPA1 cells remained intriguing. As anticipated, ONG41008 was able to greatly attenuate *NOX4* transcription along with *Collagen11α1* or *Periostin*. Furthermore, knocking down *NOX4* transcription by ONG41008 mirrored downregulation of macrophages-chemoattractant proteins such as *CCL2* and *CCL7*, suggesting that ONG41008 may affect macrophage homing to the liver. This data suggests that NOX4 plays an important role in pathogenesis of myofibroblasts. According to an interactome analysis shown in Figure 3, NOX4 seems to be functionally related to endothelin (EDN) 1, connective tissue growth factor (CTGF) and insulin-like growth factor binding proteins (IGFBP)3. HSC play a pivotal role in hepatic inflammation as well as liver fibrosis [36, 37]. Macrophage infiltration is pathologically related to steatosis or liver inflammation [38]. ONG41008 seemed to be able to block the endocytosis of CD14, one of the main LPS receptors or Myd88, disarming TLR4-driven TNFα production. Although our confocal imaging analysis may set a working hypothesis that ONG4100 may directly bind to CD14, more analytical interaction studies should be performed like DART (direct analysis in real time) as a mass spectrometry. ICC data clearly showed that LPS stimulation induced a robust endocytosis of CD14 whereas LPS plus ONG41008 may retain periplasmic distribution of CD14 in

conjunction with remarkable morphological change showing round shapes (Supplementary Figure 10). How ONG41008-mediated morphological change occurs and the morphological change affects LPS-mediated TNFα induction remain to be elucidated. No apparent change in endocytosis and morphological changes of MD-2 or NOX4 were detected (Supplementary Figure 11). Our data suggest that there are two distinct anti-fibrotic capacities associated with ONG41008; 1) inhibition of TGFβ biogenesis by dismantling of LTC via F-actin depolymerization, thereby limiting binding of TGFβ to TGFRII and 2) alteration of ECM biogenesis which is initiated in currently unknown modes, as shown in Supplementary Figure 13.

Taken together, we generated a CSD called ONG41008 that has both anti-fibrotic and anti-inflammatory capability. ONG41008 may be able to ameliorate a broad range of fibrotic diseases such as heart fibrosis, kidney fibrosis, macular fibrosis, NASH or fibrotic cancers such as pancreatic cancer. And this observation also opens a door as a powerful new therapeutic modality for treating autoreactive T cells-mediated chronic-inflammation.

Acknowledgments

We greatly appreciate Dr. HS Yoon (NTU Singapore) for scientific advices. We are thankful to D Lee (being the CTO in Osteoneurogen) for a proof reading and to all those Osteoneurogen researchers and administrative workforces who have been helping us, thereby making the current manuscript possible. This study was supported by an intramural fund from Osteoneurogen, Inc.

Competing financial interests

H-S Kim, I-K Kim, and B-S Youn retain the shares of Osteoneurogen, M-K Meang retains a stock option, and SB Kim are employed by OsteoNeuroGen. The current contents of the ONG41008 data has been granted as the subject of a Korean patent and an US patent and has been subjected to USPTO.

Author contributions

B-S Youn and H-S Kim conceived the idea. I-H Kim and B L. Seong exchanges the ideas related to therapeutic efficacy of ONG41008 to fibrotic diseases and anti-osteclastogenesis by viewing these experiments. MK Mang was largely involved in executing major experiments as well as organizing and sorting out all involved methods and materials. JY Lee played a role in TGF signaling along with ONG41008. SB Kim played a major role in trans-differentiation of HSC into pathogenic myofibroblasts. The major body of this manuscript has been exposed to public on the bioRxiv depository since September, 2019 (doi: https://doi.org/10.1101/770404).

Animal care: Mice, rats or beagle dog care was managed by the IACUC associated with Syngene International (Bangalore, India).

Footnotes:

The following abbreviated terms were mainly used in this manuscript;

CS: Chromone Scaffold

CSD: Chromone Scaffold Derivatives

IPF: Idiopathy Pulmonary Fibrosis

DHLF: Diseased Human Lung Fibroblasts from IPF patients

pMFB: pathogenic myofibroblasts

HSC: Hepatic Stellate Cells

BLM: Bleomycin-Induced Lung Fibrosis

NASH:Non-Alcoholic Steato Hepatitis

LTC: Latent TGF Complex

References

1. Meyer KC. Pulmonary fibrosis, part I: epidemiology, pathogenesis, and diagnosis. Expert Rev Respir Med. 2017;11(5):343-59.

2. Raghu G, Richeldi L, Jagerschmidt A, Martin V, Subramaniam A, Ozoux ML, et al. Idiopathic Pulmonary Fibrosis: Prospective, Case-Controlled Study of Natural History and Circulating Biomarkers. Chest. 2018;154(6):1359-70.

3. Wattacheril J, Issa D, Sanyal A. Nonalcoholic steatohepatitis (NASH) and hepatic fibrosis: Emerging therapies. Ann Rev Pharmacol Toxicol. 2018;58:649-62.

4. Bessone F, Razori MV, Roma MG. Molecular pathways of nonalcoholic fatty liver disease development and progression. Cell Mol Life Sci. 2019;76(1):99-128.

5. Marra F, Lotersztajn S. Pathophysiology of NASH: perspectives for a targeted treatment. Curr Pharm Des. 2013;19(29):5250--69.

6. Kramann R, Schneider RK. The identification of fibrosis-driving myofibroblast precursors reveals new therapeutic avenues in myelofibrosis. Blood. 2018;131(19):2111-9.

7. Ignat SR, Dinescu S, Hermenean A, Costache M. Cellular interplay as a consequence of inflammatory signals leading to liver fibrosis development. Cells. 2020;9(2):E461.

8. Lemoinne S, Friedman SL. New and emerging anti-fibrotic therapeutics entering or already in clinical trials in chronic liver diseases. Curr Opin Pharmacol 2019;49:60-70.

9. Miao CM, Jiang XW, He K, Li PZ, Liu ZJ, Cao D, et al. Bone marrow stromal cells attenuate LPS-induced mouse acute liver injury via the prostaglandin E 2-dependent repression of the NLRP3 inflammasome in Kupffer cells. Immunol Lett. 2016;179:102-13.

10. Dixon RA, Pasinetti GM. Flavonoids and isoflavonoids: From plant biology to agriculture and neuroscience. Plant Physiol. 2010;154(2):453-7.

11. Stapleton AE, Walbot V. Flavonoids can protect maize DNA from the induction of ultraviolet radiation damage. Plant Physiol. 1994;105(3):881-9.

12. Leyva-López N, Gutierrez-Grijalva EP, Ambriz-Perez DL, Heredia JB. Flavonoids as cytokine modulators: A possible therapy for inflammation-related diseases. Int J Mol Sci 2016;17(6):921.

13. Emami S, Ghanbarimasir Z. Recent advances of chroman-4-one derivatives: synthetic approaches and bioactivities. Eur J Med Chem 2015;93:539-63.

14. Gacche RN, Meshram RJ, Shegokar HD, Gond DS, Kamble SS, Dhabadge VN, et al. Flavonoids as a scaffold for development of novel anti-angiogenic agents: An experimental and computational enquiry. Arch Biochem Biophys 2015;577-578:35=48.

15. Kim JY, Lee MS, Baek JM, Park J, Youn BS, Oh J. Massive elimination of multinucleated osteoclasts by eupatilin is due to dual inhibition of transcription and cytoskeletal rearrangement. Bone Rep. 2015;3:83-94.

16. Troeger JS, Mederacke I, Gwak GY, Dapito DH, Mu X, Hsu CC, et al. Deactivation of hepatic stellate cells during liver fibrosis resolution in mice. Gastroenterology. 2012;143(4):1073-83.

17. Wang Y, Brooks PJ, Jang JJ, Silver A, Arora PD, McCulloch CA, et al. Role of actin filaments in fusopod formation and osteoclastogenesis. Biochim Biophys Acta. 2015;1853(7):1715-24.

18. Robertson IB, Horiguchi M, Zilberberg L, Dabovic B, Hadjiolova K, Rifkin DB. Latent TGF-β-binding proteins. Matrix Biol. 2015;47:44-53.

19. Makarev E, Izumchenko E, Aihara F, Wysocki P, Zhu Q, Buzdin A, et al. Common pathway signature in lung and liver fibrosis. Cell Cycle. 2016;15(13):1667-73.

20. Wang Y, Yella J, Chen J, McCormack FX, Madala SK, Jegga AG. Unsupervised gene expression analysis identify IPF-severity correlated signatures, associated genes and biomarkers. BMC Pulm Med. 2017;17:133.

21. Mullenbrock S, Liu F, Szak S, Hronowski X, Gao B, Juhasz P, et al. Systems analysis

of transcriptomic and proteomic profiles identifies novel regulation of fibrotic programs by miRNAs in pulmonary fibrosis fibroblasts. Genes (Basel). 2018;9(12):pii: E588.

22. Hoff CR, Perkins DR, Davidson JM. Elastin gene expression is upregulated during pulmonary fibrosis. Connect Tissue Res. 1999;40(2):145-53.

23. Chen W, Yan X, Xu A, Sun Y, Wang B, Huang T, et al. Dynamics of elastin in liver fibrosis: Accumulates late during progression and degrades slowly in regression. J Cell Physiol. 2019;234(12):22613-22.

24. Singh A, Koduru B, Carlisle C, Akhter H, Liu RM, Schroder K, et al. NADPH oxidase 4 modulates hepatic responses to lipopolysaccharide mediated by Toll-like receptor-4. Sci Rep. 2017;7(1):14346.

25. Kakino S, Ohki T, Nakayama H, Yuan X, Otabe S, Hashinaga T, et al. Pivotal role of TNF-α in the development and progression of nonalcoholic fatty liver disease in a murine model. Horm Metab Res. 2018;50(1):80-7.

26. Grant R, Nguyen KY, Ravussin A, Albarado D, Youm YH, Dixit VD. Inactivation of C/ebp homologous protein-driven immune-metabolic interactions exacerbate obesity and adipose tissue leukocytosis. J Biol Chem. 2014;289(20):14045-55.

27. Sun B, Wang X, Ji Z, Wang M, Liao YP, Chang CH, et al. NADPH Oxidase-Dependent NLRP3 Inflammasome activation and its important role in lung fibrosis by multiwalled carbon nanotubes. Small. 2015;11(17):2087-97.

28. Zhang LL, Huang S, Ma XX, Zhang WY, Wang D, Jin SY, et al. Angiotensin(1-7) attenuated Angiotensin II-induced hepatocyte EMT by inhibiting NOX-derived H2O2-activated NLRP3 inflammasome/IL-1β/Smad circuit. Free Radic Biol Med. 2016;97:531-43.

29. Cheng Z, Taylor B, Ourthiague DR, Hoffmann A. Distinct single-cell signaling characteristics are conferred by the MyD88 and TRIF pathways during TLR4 activation. Science Signaling. 2015;8(385):ra69.

30. Monteiro PA, do Prado WL, Dos Santos Tenório TR, Tomaz LM, St-Pierre DH, Lira FS. Immunometabolic Changes in Hepatocytes Arising from Obesity and the Practice of Physical Exercise. Curr Pharm Des. 2018;24(27):3200-9.

31. Saito K, Uebanso T, Maekawa K, Ishikawa M, Taguchi R, Nammo T, et al. Characterization of hepatic lipid profiles in a mouse model with nonalcoholic steatohepatitis and subsequent fibrosis. Sci Rep. 2015;5:12466.

32. Owona BA, Abia WA, Moundipa PF. Natural compounds flavonoids as modulators of inflammasomes in chronic diseases. Int Immunopharmacol. 2020;84:106498.

33. Kim HS, Yoon YM, Meang MK, Park YE, Lee JY, Lee TH, et al. Reversion of in vivo fibrogenesis by novel chromone scaffolds. EBioMedicine. 2019;39:484-96.

34. Karin D, Koyama Y, Brenner D, Kisseleva T. The characteristics of activated portal fibroblasts/myofibroblasts in liver fibrosis. Differentiation. 2016;92(3):84-92.

35. Nonnenmacher Y, Hiller K. Biochemistry of proinflammatory macrophage activation. Cell Mol Life Sci 2018;75(12):2093-109.

36. Weiskirchen R, Tacke F. Cellular and molecular functions of hepatic stellate cells in inflammatory responses and liver immunology. Hepatobiliary Surg Nutr. 2014;3(6):344-63.

37. Higashi T, Friedman SL, Hoshida Y. Hepatic stellate cells as key target in liver fibrosis. Adv Drug Deliv Rev. 2017;121:27-42.

38. Koyama Y, Brenner DA. Liver inflammation and fibrosis. J Clin Invest. 2017;127(1):55-64.

39. Ihn H, Kim K, Cho H, EK P. Pentamidine inhibits titanium particle-induced osteolysis in vivo and Receptor Activator of Nuclear factor-kB Ligand-mediated osteoclast differentiation in vitro. Tissue Eng Reg Med. 2019;16(3):265-73.

Figure legends

Fig. 1. ONG41008 inhibits trans-differentiation of mouse HSC into pMFB. (A) ICC was performed for α-SMA on ONGHEPA1, a mouse HSC line, after 24hrs treatment with medium, TGFβ (2.5ng/ml), or TGFβ plus ONG41008 (25μM) and cell reactivities were observed under florescent microscope. *Periostin*, *Collagen1α1*, *Collagen11α1* mRNA levels were measured by qPCR along with ICC. (B) Kinetics of TGFβ-induced SMAD or ERK phosphorylation in presence of ONG41008 was conducted by western blot using the cell lysates of ONGHEPA1 treated with TGFβ in the presence of ONG41008 at various time points; 0, 5, 15, 30, 45, 60, 120 mins. (C) Actin-Phalloidin staining to test actin depolymerization was explored. ONGHEPA1 cells were treated with ONG41008, Pirfenidone, or Nintedanib in the presence of TGFβ as compared to DMEM and was subjected to microscopic observation. (D) *In vitro* actin polymerization and (E) depolymerization assay. Actin polymerization activity and amount of depolymerization were measured in kinetic mode fluorometer at different concentration of ONG41008. Statistical significance was calculated by Student's t-test. *, $P < 0.05$, **, $P<0.01$.

Fig. 2. Change of latent TGFβ complex (LTC)–associated proteome expression in ONG41008-treated DHLF and ONGHEPA1 cells (A) DHLF were stained for LTBP1 (green), LAP1 (green), LTBP4 and DAPI (nuclei, blue). LTBP1 and LAP1, but not LTBP4, were significantly down-regulated by ONG41008. (B) ONGHEPA1 cells were stained for F-actin (phalloidin, red), mLTBP1 (green), mLTBP4 (green), mLAP1 (green), integrin α5β3 and DAPI (nuclei, blue).

Fig. 3. Transcriptomic analysis shows a set of genes, seventy-seven, called TGFβ-induced fibrosis-inducing genes (FIGS) significantly downregulated by ONG41008 (A) List of seventy-seven ONG41008 suppressible FIGS. (B) Interactome study using the STRING

database based on the above listed seventy-seven FIGS. Of those, twenty-eight genes-encoded proteins appeared to be isolated from the major interactome and thus were deleted to better visualize connectivity.

Fig. 4. NOX4, CCL2 and CCL7 are inducible by TGFβ and blocked by ONG41008. (A) qPCR for analysis of gene expression of Collagen*11α1, Periostin* and *NOX4* in TGFβ treated ONGHEPA1 at various time points; 0, 6, 9, 12, 24 hr. (B) ICC for NOX4 on ONGHEPA1 and (C) DHLF incubated 24hrs in medium, TGFβ, or TGFβ plus ONG41008. With the same treatment conditions, (D) ROS assay using DCFDA on ONGHEPA1 and (E) qPCR for *NOX4, CCL2, CCL7* on ONGHEPA1 were performed.

Fig. 5. ONG41008 reverses myofibroblasts into an intermediate non-myofibroblasts. (A) Trans-differentiation was conducted for 24 hr. Myofibroblasts were washed with buffer and were restimulated with TGFβ plus ONG41008 for 24 hr. The resulting intermediate cells were kept incubated with TGFβ alone for 72 hr. Morphological changes were monitored under a phase-contrast microscope. (B) Fibrogenic interactome in ONGHEPA1was acquired by differential stimulations; medium, TGFβ or TGFβ plus ONG41008. Collagen hubs, cell adhesins hubs and chemokines hubs are denoted by arrows. Intermediate cells were subjected to RNA-seq for establishing a reversion interactome, and two distinct interactomes coexist; 1) residual fibrogenic interactome comprising of Col6α3, Col11α1, Coll3α1, and Spp1 and 2) an evident nuclear reprogramming interactome.

Fig. 6. Anti-fibrotic effect of ONG41008 in bleomycin-induced lung fibrosis model. (A and B) Lung collagen and hydroxyproline levels were measured after pirfenidone or different dosages of ONG41008 (10, 25, 50mpk) oral administration in BLM therapeutic model. Percent

inhibition relative to Vehicle control are presented in orange with average measurement. (C) Lung sections were analyzed by Masson's Trichome staining for BLM therapeutic model and αSMA staining was conducted. Percent αSMA-positive area was measured and statistical significance was calculated by Student's t-test. ***, $P < 0.001$, relative to Sham. $, $P < 0.05$, $$$, $P < 0.001$ relative to vehicle control.

Fig. 7. Inhibition of LPS-inducible genes by ONG41008 in LPS-stimulated RAW264.7 cell. RAW264.7 cells were stimulated with LPS (100ng/ml) or LPS plus ONG41008 (25μM, 50μM) for 24hrs and mRNA expression for inflammatory markers were measured by qPCR.

Fig. 8. Inhibition of CD14 trafficking by ONG41008 in LPS-stimulated RAW264.7 cell. (A) Confocal imaging analysis for CD14 in RAW264.7 cells which were incubated in medium, LPS or LPS plus ONG41008. CD14 or Myd66 cellular trafficking was monitored via confocal imaging. (B) An interactome operational for LPS-ONG41008 axis in RAW264.7 cells revealed that TNFα turned out to be the central hub of the interactome.

Fig. 9. Anti-fibrotic effect of ONG41008 in NASH and NAFLD in STAM mouse model. (A and B) H&E staining of liver sections of STAM mouse were analyzed after oral administration pf Telmisartan, OCA or ONG41008. Liver samples were photographed after hepatectomy. (C) NAFLD activity score charted for ONG41008 and controls. Statistical significance was calculated by Student's t-test.

Materials and Methods

Cell culture and reagents

DHLFs were purchased from Lonza (Basel, Switzerland) and cultured in fibroblast growth medium (FBM, Lonza, Walkersville, MD, USA). Recombinant human TGFβ and PDGF were obtained from Peprotech (Rocky Hill, CT, USA) and used at a final concentration of 5 ng/ml. Chemically synthesized ONG41008 was obtained from Syngene International Ltd. (Bangalore, India), dissolved at a stock concentration of 50 mM in DMSO, and stored in aliquots at -20°C. DMSO with according concentration was used as control. RAW264.7 cell line was purchased from Korean Cell Line Bank (Seoul, Korea) and cultured in RPMI supplemented with 10% FBS and 1% P/S (Welgene, Seoul, Korea). LPS was purchased from Sigma and used at final concentration of 100 ng/ml.

Effects of drugs on bleomycin-induced lung tissue fibrosis

C57BL/6J mice were anesthetized by inhalation of 70% N_2O and 30% O_2 gas containing 1.5% isoflurane. Fifty microliters of bleomycin solution in distilled water was directly injected into the lungs, all at once, via the aperture. Immediately after injection, the mice were allowed to recover from the anesthetic, and then housed in normal cages. Bleomycin (0.03U BLM in 50μl saline) was administered once using a visual instillobot. Twelve days after the administration of bleomycin, ONG41008 was forcibly nasally administered via a micropipette, once a day (five times a week) for 1 week. ONG41008 was dissolved in DPBS buffer (containing 1% DMSO), and 1 ml/kg was administered based on the most recent body weight. For 2 to 3 days after administration of ONG41008, mice were monitored for toxic symptoms or death, but no abnormal symptoms were observed. Three mice per test group were selected, and their lung tissues were excised. The lung tissues were stained with Masson's trichrome and observed under a microscope. The degree of fibrosis of

the lungs was assessed by an independent pathologist using the Ashcroft scoring system. Results were expressed as mean values and standard deviations. One hour before sacrifice, a final dose of ONG41008 or pirfenidone was administered for plasma or lung PK. The bleomycin-treated mice exhibited a rapid decline in weight, but the sham control behaved normally. ONG41008- or pirfenidone-administered mice exhibited weight gain from day 3 onward. Control and ONG41008-treated mice data were compared using Student's *t*-test. "Differences between samples were considered statistically significant when $p<0.05$.

RNA-seq processing, differential gene expression analysis, and interactome analysis

Processed reads were mapped to the *Mus musculus* reference genome (Ensembl 77) using Tophat and Cufflink with default parameters. Differential analysis was performed using Cuffdiff using default parameters. Further, FPKM values from Cuffdiff were normalized and quantitated using the R Package Tag Count Comparison (TCC) to determine statistical significance (e.g., P values) and differential expression (e.g., fold changes). Gene expression values were plotted in various ways (i.e., Scatter, MA, and Volcano plots), using fold-change values, using an R script developed in-house. The protein interaction transfer procedure was performed using the STRING database with the differentially expressed genes. A 60 Gb sequence was generated, and 10,020 transcripts were read and compared. The highest-confidence interaction score (0.9) was applied from the *Mus musculus* species, and information about interacts were obtained based on text mining, experiments, and databases (http://www.string-db.org/). Due to company information sake the above detailed RNA-Seq or interactome data interpretation would be limited but essential data sufficiently supporting our assertion were provided.

Reverse transcriptase PCR and real-time PCR

Cells cultured in either 12 or 24-well plates were washed twice with cold PBS and harvested using TaKaRa MiniBEST Universal RNA extraction kit (Takara, Japan). RNA was purified using the same kit according to manufacturer's protocol. RNA was reverse-transcribed using the cDNA Synthesis Kit (PCRBio Systems, London, UK). Synthesized cDNA was amplified with StepOne Plus (Applied Biosystems, Life Technologies) and 2× qPCRBio Probe Mix Hi-ROX (PCRBio). Comparisons between mRNA levels were performed using the ΔΔCt method, with GAPDH as the internal control.

ELISA and immunoblotting

Mouse TNFα Quantikine ELISA kit was purchased from R&D systems (Minneapolis, MN, USA). Raw264.7 cell was seeded at 1 x 10^5 in 12 well cell culture plate and incubated O/N. The cells were then treated with LPS (100ng/ml) and ONG41008 at the indicated concentrations. Balancing amount of DMSO was added to each treatment condition. After 24HRs of treatment supernatant from each was collected for ELISA. The assay was performed according to the manufacturer's manual. For three repeat experiment standard curve was made each time to calculate TNFα concentration. DHLF at a density of 2x10^5cells/ml were seeded onto 24well plate, followed by treatment with TGFβ (2.5ng/ml) and TGFβ (2.5ng/ml) plus various concentrations of ONG41008. After 24 hr, the supernatants were collected and performed with human elastin ELISA kit (Abcam, ab239433) following the manufacturer's protocol. For western blotting, antibodies for CD14, MD-2, P62, GAPDH were purchased from Abcam (Cambridge, UK), MyD88, TLR4 from R&D systems, NOX4 (14347-1-AP) from Proteintech (Rosemont, IL, USA), and LC3 A/B, pSMAD-2, pSMAD-3, SMAD2/3, pERK 1/2, ERK 1/2 from Cell Signaling Technology (Danver, MA, USA). All antibodies were diluted to 1:1000 v/v in 5% BSA in DPBS (Welgene).

Immunocytochemistry

Cells were fixed using 4% paraformaldehyde, permeabilized with 0.3% TritonX100, blocked and incubated with 1:500 anti α-Smooth Muscle Actin (Young In Frontier, Korea), 1:500 Actin Phalloidin (Thermo Fisher, USA), 1:500 anti-LTBP1 (Aviva Systems Biology, San Diego, USA), 1:500 anti- LTBP4 (Aviva Systems Biology), 1:500 anti-LAP1 (Abcam), 1:500 anti-integrin α5β3 (biorbyt, Cambridge, UK), 1:500 anti-NOX4 (Proteintech), 1:500 anti-CD14 (Abcam), 1:500 anti-MyD88 (R&D systems), 1:500 anti-TLR4 (R&D systems) or 1:500 anti-MD-2 (Abcam) antibodies and 1:200 FITC conjugated secondary antibody (Young In Frontier) and imaged with fluorescence microscope EVOS® FL (Thermo). Nuclei were stained with DAPI

Confocal imaging

Cells were fixed with 4% paraformaldehyde, permeabilized with 0.4% Triton X100, blocked with 1% BSA and incubated with anti-CD14 (1:500, Abcam), anti-Myd88 (1:500, R&D systems) for overnight at 4ºC. After FITC conjugated secondary antibody incubation (1:200, Ab Frontier) for 1 hr at 37ºC, images were acquired using Laser scanning confocal microscope (Carl Zeiss LSM700) with 63x oil immersion lens. Confocal images were analyzed with Zen black software.

ROS staining

Intracellular production of ROS was detected after stimulation of ONGHEAPA1 cells with TGFβ (5ng/ml) or TGFβ plus ONG41008 (50μM). Cells were incubated with 10μM H2DCFDA (Abcam) for 1 hr in dark at 37ºC. The cells were then examined with fluorescence microscope EVOS® FL (Thermo).

Induction of osteoclast differentiation

Animal experimental protocols were approved by the institutional Animal Care and Use Committee at Yonsei University Wonju College of Medicine (Identification code: YWC-200325-1) and procedures were performed in accordance with the guidelines of the National Institutes of Health's Guide for the Care and Use of Laboratory Animals. Bone marrow mononuclear cells and marrow-derived macrophages were derived as previously described [39]. Briefly, mouse bone marrow cells were harvested from femurs and tibias from 8-week-old Balb/c mice and cultured overnight on 100-mm dishes in α-MEM(WelGENE Inc., Republic of Korea) supplemented with 10% fetal bovine serum (FBS) and penicillin/streptomycin. Floating cells were collected and further cultured in the presence of M-CSF (30 ng/ml) for 4 days to generate bone marrow-derived macrophages (BMM). To induce osteoclast differentiation, BMM were stimulated with 100 ng/mL RANKL and 30 ng/mL M-CSF in the presence or absence of ONG41008.

Actin polymerization/depolymerization assay

Actin Polymerization/Depolymerization Assay Kit (Abcam, ab239724) was used for both assays. For actin polymerization assay mixture of; actin, buffer, and test samples were placed in 96 plate well in order of supplemented Buffer G (2μM ATP, 5μM DTT), actin, and test samples. As test samples, Buffer G was used as background control, DMSO as positive control, and ONG41008 in DMSO with concentration range from 25 to 100μM were used. The mixtures in each well were then pipetted thoroughly to mix and incubated in dark, at room temperature, for 15 min. After incubation the polymerization activation buffer, supplemented 10X Buffer P (10mM ATP) was added into each well and thoroughly pipetted. For actin depolymerization assay; Buffer G (2μM ATP, 5μM DTT), supplemented 10X Buffer P (10mM ATP), and actin were placed in 96 plate well in listed order and pipetted to mix thoroughly. The

mixture was incubated in dark, at room temperature, for 1 hr for polymerization to take effect. After the incubation test samples, DMSO as negative control and ONG41008 at concentration from 25 to 100μM, were added to each appropriate well and pipetted thoroughly. Florescence of both actin polymerization and depolymerization assay were measured with Florescence/Luminescence Analyzer Hidex Sense at florescence Ex/Em 355/405nm (range 5~10nm) in kinetic mode for 2 hr (180 cycles).

Supplemental information

Figure legends

Suppl. Fig. S1. Non-GLP toxicokinetic of ONG41008. (A) ONG41008 was orally administered into mice. Three mice per test group were studied, and their plasma were exercised. (B) Non-GLP single injection oral PK was studied using beagle dogs.

Suppl. Fig. S2. Tissue PK of ONG41008 study. Mice and rat were orally injected ONG41008 at 100mpk. Concentration of drug exposure was detected plasma, lung, liver and kidney tissue at 5 min, 15 min, 30 min, 1 hr and 2 hr time point.

Suppl. Fig. 3. ONG41008 inhibits prefibrotic genes expression in DHLF (A) ICC was performed for α-SMA after 24 hr treatment with medium, TGFβ, TGFβ plus ONG41008, and was observed under florescent microscope. *Collagen11α1*, *Collagen1α1* and *Periostin* mRNA level was measured by qPCR in parallel to ICC set.

Suppl. Fig. 4 ONG41009 inhibits RANKL-induced multi-nucleated osteoclasts differentiation *in vitro*. Murine bone marrow-derived macrophages (BMMs) were cultured with RANKL and M-CSF (10 ng/mL) and (20 ng/mL) in the presence or absence of ONG40118 (25 μM). Scale bar = 500 μm.

Suppl. Fig. S5. Schematic of fibrosis-inducing gene selection process. Transcriptomic analysis from DHLF treated with TGFβ or TGFβ plus ONG41008 shows 77 TGFβ-induced

fibrosis-inducing genes (FIGS) significantly downregulated by ONG41008. Differential expression was explored with $p< 0.005$.

Suppl. Fig. S6. ONG41008 inhibits ELN production in DHLF. (A) IC50 of ONG41008 for *Eln* mRNA expression was determined by qPCR. (B) Culture supernatants from DHLF treated with TGFβ or TGFβ plus ONG41008 were examined for ELN protein levels by ELISA. **P < 0.001 and *P <0.05 relative to vehicle control were determined by Student's t-tests.

Suppl. Fig. S7. Transcriptomic analysis and establishment of a ONG41008-specific interactome in the mouse liver RNA-seq was performed by using total RNAs from ONGHEPA1 treated by control, TGFβ, or TGFβ + ONG41008. Differential expression was explored with $p< 0.005$. An interactome study using STRING based on sixty-one FIGS derived from RNA-Seq. Representative interactomes are denoted by colored ovals.

Suppl. Fig. S8. ONG41008 had positive effects against lung fibrosis in BLM prevention model. (A) Lung collagen and hydroxyproline levels measured after treatment with pirfenidone or 10, 25, or 50 mg/kg ONG41008 in the BLM prevention model. Percent inhibition relative to vehicle control is shown in orange characters, with average measurements in gray. (B) Masson's Trichome staining of lung sections in the BLM prevention model. Representative magnification, × 200 (C) Ashcroft fibrosis score on day 21. ***P < 0.001, relative to Sham, and $P < 0.05, $$$P < 0.001 relative to vehicle control by Student's t-tests.

Suppl. Fig. S9. ONG41008 inhibits LPS-induced TNFα expression in RAW264.7 cells. (A) RAW264.7 cells were treated with different concentrations of LPS and/or ONG41008 for 12

hr and levels of TNFα mRNA were analyzed by quantitative RT-PCR. (B) Supernatants of cultured RAW264.7 treated with LPS and/or ONG41008 were collected and ELISA was performed to measure the expression of TNFα. Data are presented as the mean ± standard deviation (n=3).

Suppl. Figure S10. Plasma membrane sequestration of CD14 by ONG41008 in LPS-stimulated RAW264.7 cells. RAW264.7 cells were cultured overnight with LPS plus ONG41008. FITC-labeled CD14 (Green) antibody was reacted with RAW264.7 cells. DAPI was used to stain nuclei (blue). The fluorescence of CD14 was detected with 40X objective using EVOS® FL microscope. CD14 was expressed in plasma membrane of unstimulated RAW264.7 cell and ONG41008 inhibited the recycling of CD14 in LPS-stimulated RAW264.7 cells.

Suppl. Figure S11. The fluorescence levels of MD-2, TLR4, MyD88 and NOX4 was consistent. RAW 264.7 cells were stimulated with Medium, LPS or LPS plus ONG41008 for 24 hr. FITC-labeled Myd88 antibody (1/500), FITC-labeled TLR4 antibody (1/500), FITC-labeled MD-2 antibody (1/500) or FITC-labeled NOX4 antibody (1/500) was immuno-stained with permeabilized RAW 264.7 cells. Nuclei were presented by DAPI (Blue). The image was captured with a 40X objective using EVOS® FL microscope.

Suppl. Figure S12 Signs of hepatic steatosis, lobular inflammation and hepatocyte ballooning in each condition in STAM mice treated with control, ONG41008, Telmisartan, or OCA were pictured and denoted.

Suppl. Figure S13. Potential mechanism of ONG41008 action in the treatment of organ

fibrosis. Major one destroys actin stress filaments via depolymerization of F-actin, leaving latent TGFβ complex dismantled. Inability of TGFβ binding to TGFβ II or I signaling receptor is unable to generate canonical or noncanonical TGFR signaling leading to attenuation of type 2 EMT. Furthermore, ONG41008 blocks phosphorylation of SMAD2/3. These two acting mechanisms may be responsible for efficiently disarming proliferation of or collagen or hydroxyproline production of myofibroblasts. Reversion and induction of autophagy independently of TGFβ may play an important role in giving rise to beneficial features, suggesting that it may also prevent fibrosis and promote cellular homeostasis such as cell survival, anti-steatosis or lowering insulin resistance. We suppose that these two working mechanisms might be initiated from ECM.

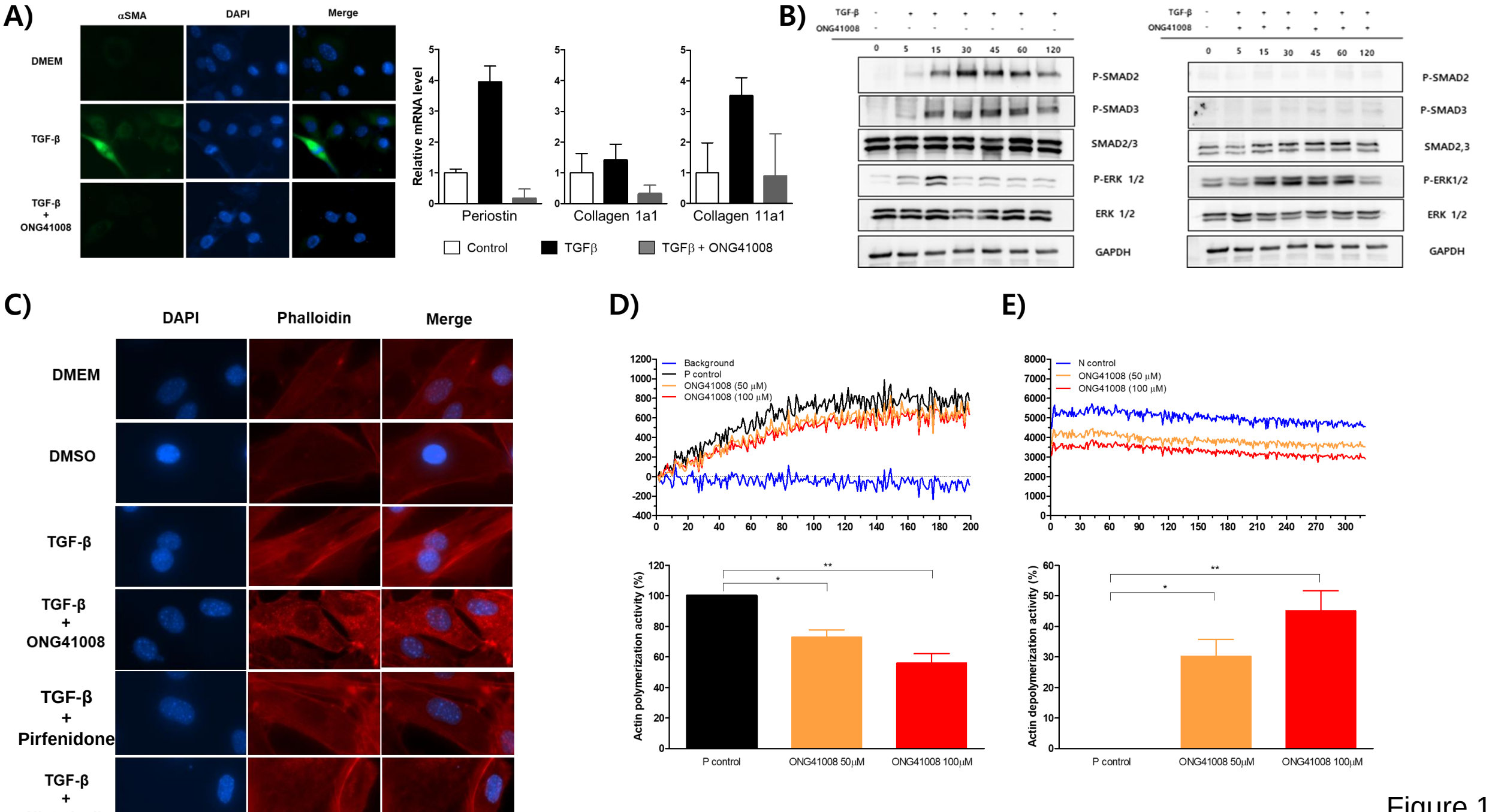
A)
αSMA
DAPI
Merge
DMEM
TGF-β
TGF-β + ONG41008
Relative mRNA level
Periostin
Collagen 1a1
Collagen 11a1
Control
TGFβ
TGFβ + ONG41008
B)
TGF-β
ONG41008
0 5 15 30 45 60 120
P-SMAD2
P-SMAD3
SMAD2/3
P-ERK 1/2
ERK 1/2
GAPDH
P-SMAD2
P-SMAD3
SMAD2,3
P-ERK1/2
ERK 1/2
GAPDH
C)
DAPI
Phalloidin
Merge
DMEM
DMSO
TGF-β
TGF-β + ONG41008
TGF-β + Pirfenidone
TGF-β + Nintedanib
D)
Background
P control
ONG41008 (50 μM)
ONG41008 (100 μM)
Actin polymerization activity (%)
P control
ONG41008 50μM
ONG41008 100μM
E)
N control
ONG41008 (50 μM)
ONG41008 (100 μM)
Actin depolymerization activity (%)
P control
ONG41008 50μM
ONG41008 100μM

Figure 1

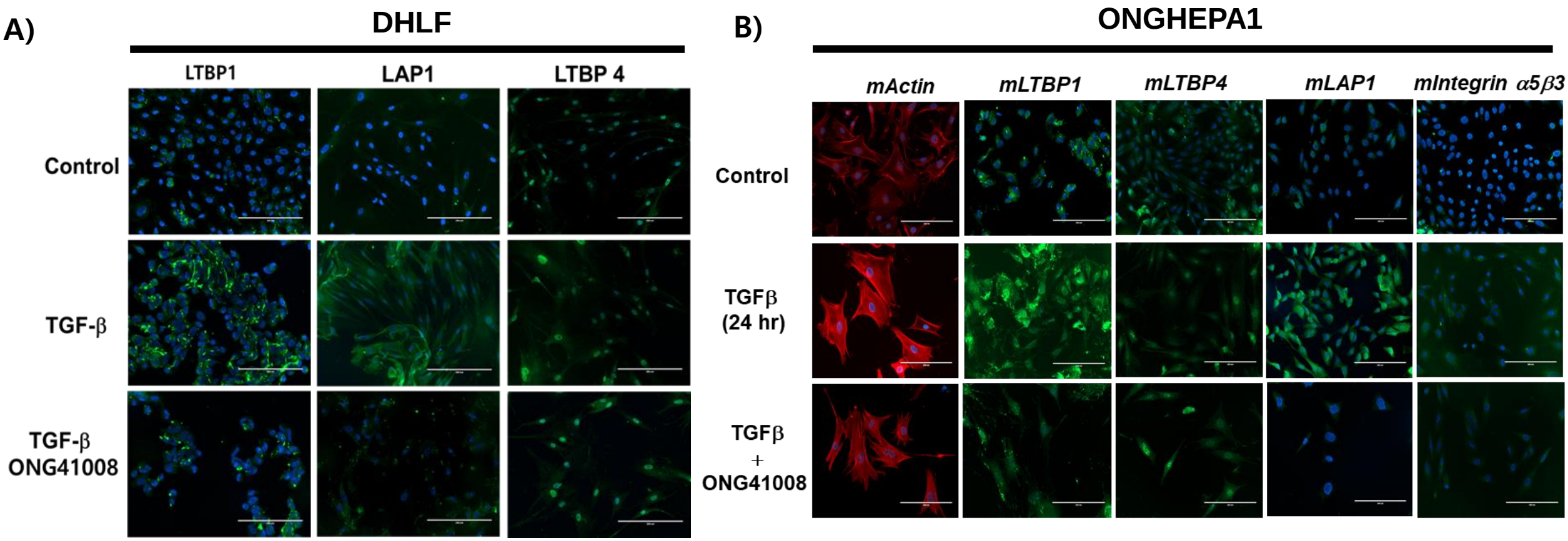
A)
DHLF
LTBP1
LAP1
LTBP 4
Control
TGF-β
TGF-β
ONG41008
B)
ONGHEPA1
mActin
mLTBP1
mLTBP4
mLAP1
mIntegrin α5β3
Control
TGFβ
(24 hr)
TGFβ
+
ONG41008

Figure 2

A)

Human DHLF regulated by ONG41008 via RNA-Seq / p< 0.005

EPHB2
LEPRE1
KIF26B
PLXDC2
ANKRD1
POSTN
XYLT1
FAM101B
CDH2
PXDN
COL7A1
PCDH10
CDH6
SPOCK1
EDN1
CTGF
IGFBP3
LRRC17
PLAT
CTHRC1
COL5A1
NEGR1
VDR
COL4A1
TPM1
COL11A1
FAM46A
EDIL3
ELN
DKK1
TCF4
PLOD2
NEK7

PAWR
APCDD1L
GALNT10
PKP1
PXDC1
GJA1
NTM
SH3PXD2A
LEPREL4
PODXL
PSAT1
NOX4
RP11-180C1.1
FBLN5
ADAM19
MRC2
COL1A1
WWTR1
LOX
ITGB5
HHAT
KSR1
HMCN1
GATA6
CDK6
P4HA2
EFEMP1
ALDH1L2
SLC38A5
SEMA7A
FIBCD1
NCOA3
P4HA1
ATP10A
PYCR1
RNF152
HAPLN1
COL5A2
DGKI
HYOU1
ASXL3
SERPINH1
SOX2-OT

B)

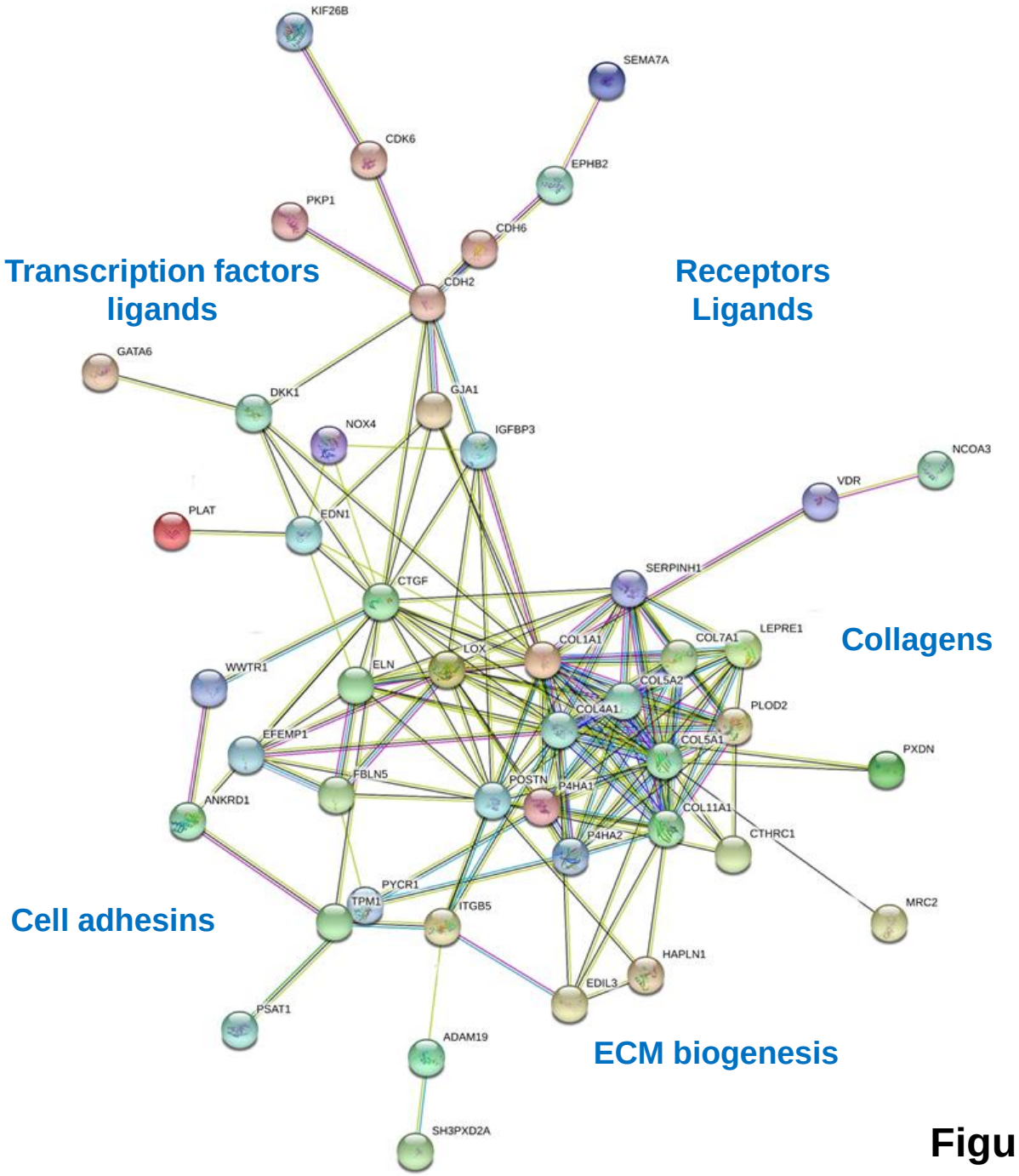

Figure 3

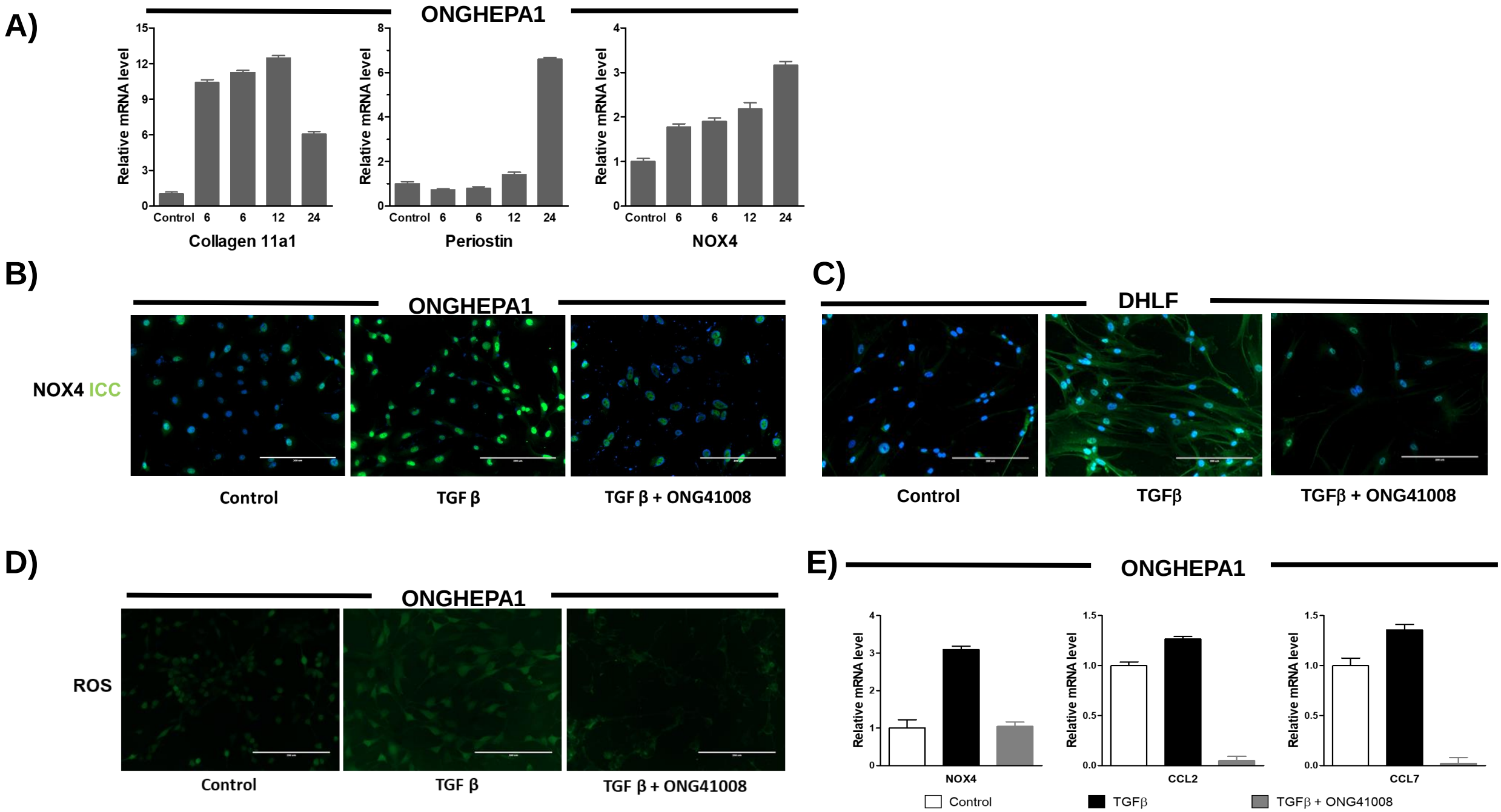
A)
ONGHEPA1
Relative mRNA level
Control 6 6 12 24
Collagen 11a1
Periostin
NOX4
B)
ONGHEPA1
NOX4 ICC
Control
TGF β
TGF β + ONG41008
C)
DHLF
Control
TGFβ
TGFβ + ONG41008
D)
ONGHEPA1
ROS
Control
TGF β
TGF β + ONG41008
E)
ONGHEPA1
Relative mRNA level
NOX4
CCL2
CCL7
Control
TGFβ
TGFβ + ONG41008

Figure 4

A)

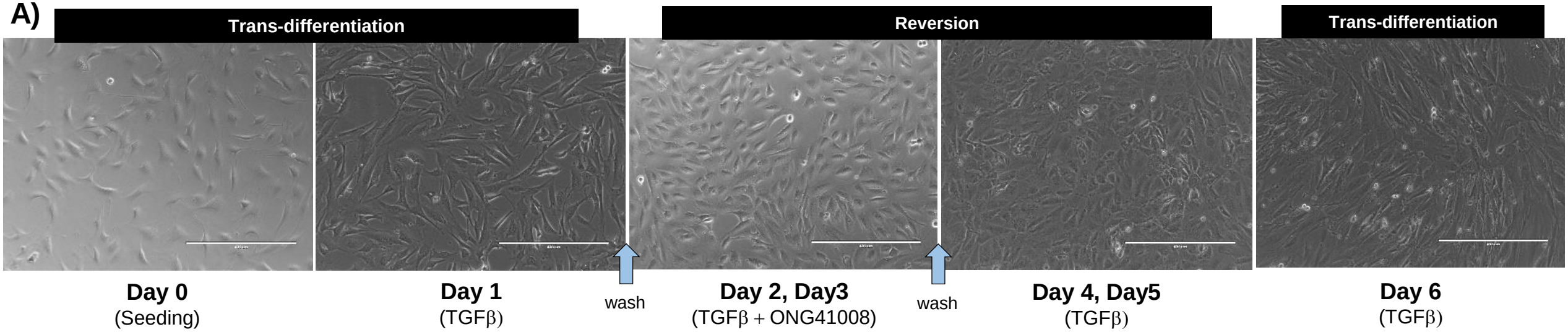

B)

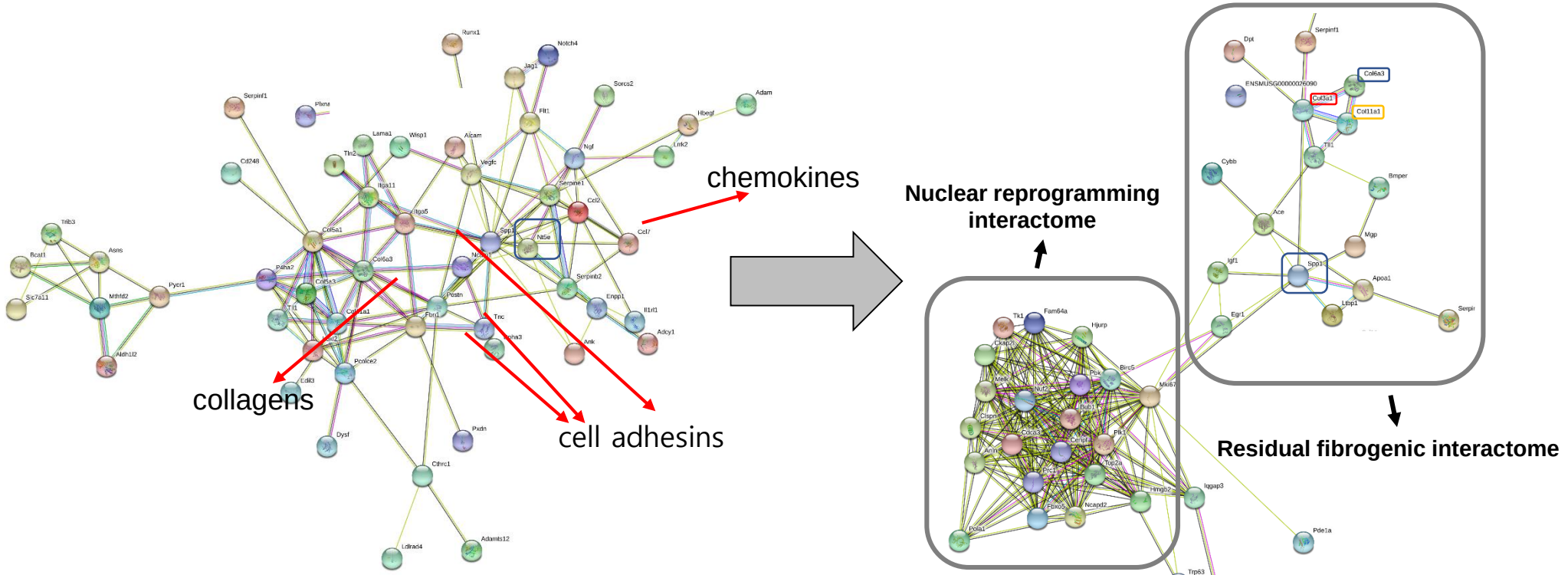

Fibrogenic Interactome
(ONGHEPA1(HSCs) → Myofibroblasts)

Reversion Interactome
(Myofibroblast → Intermediate cells)

Figure 5

A)

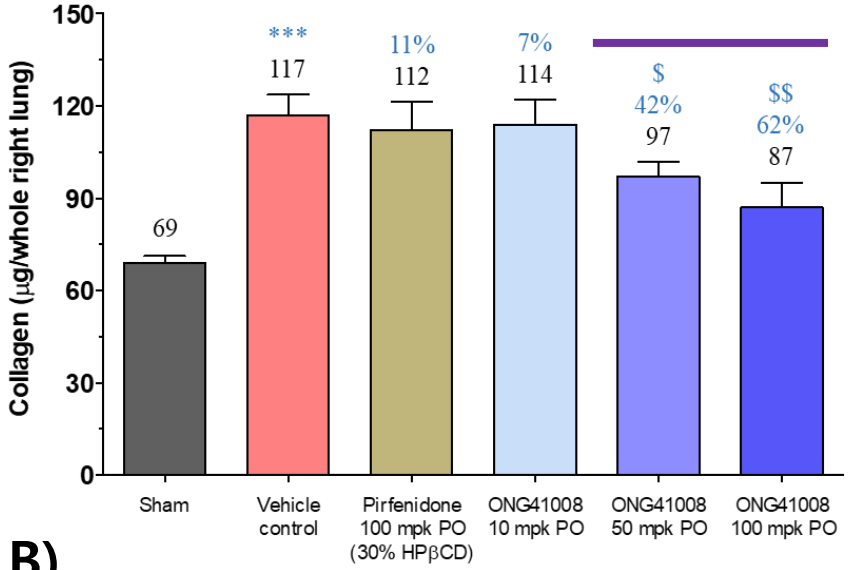

B)

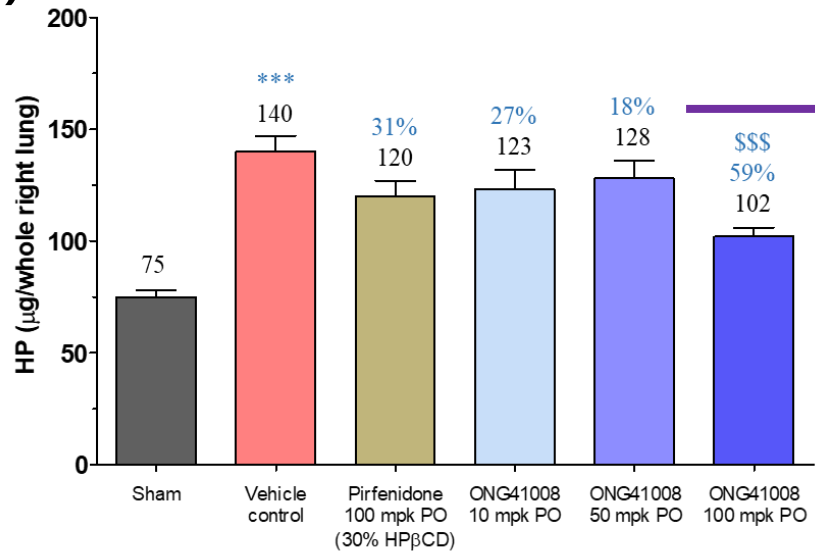

C)

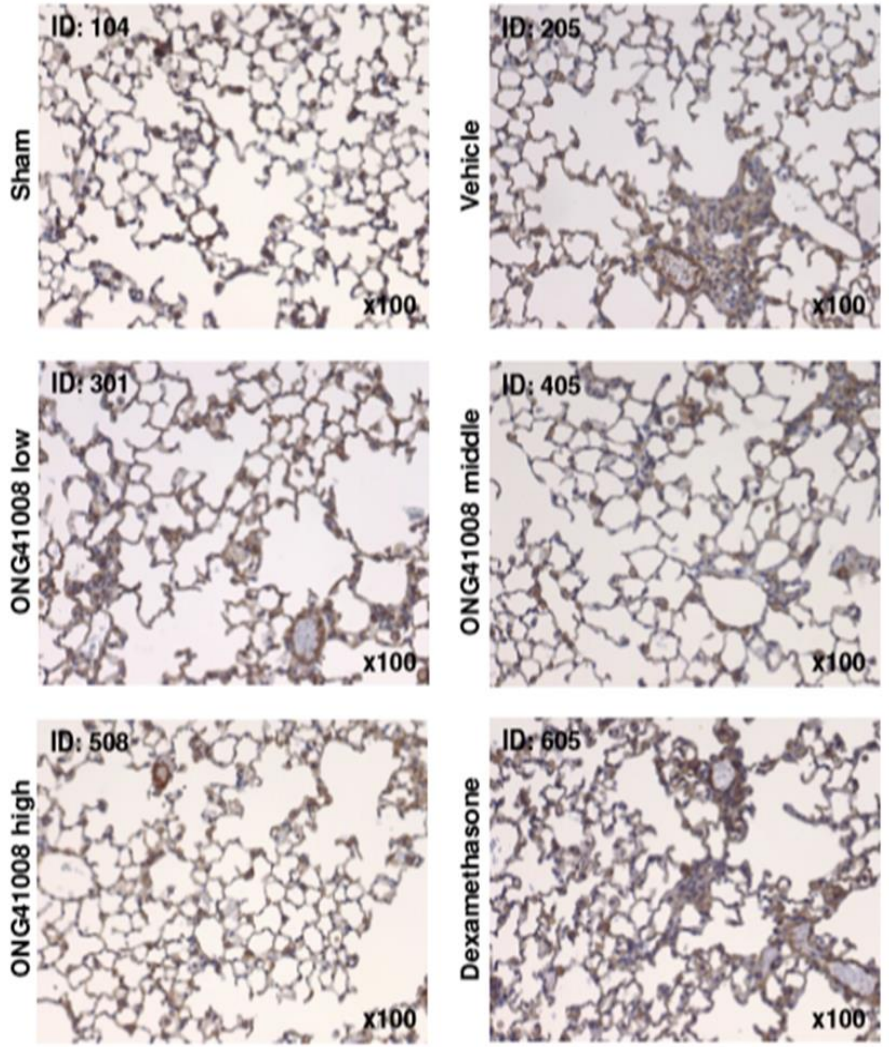

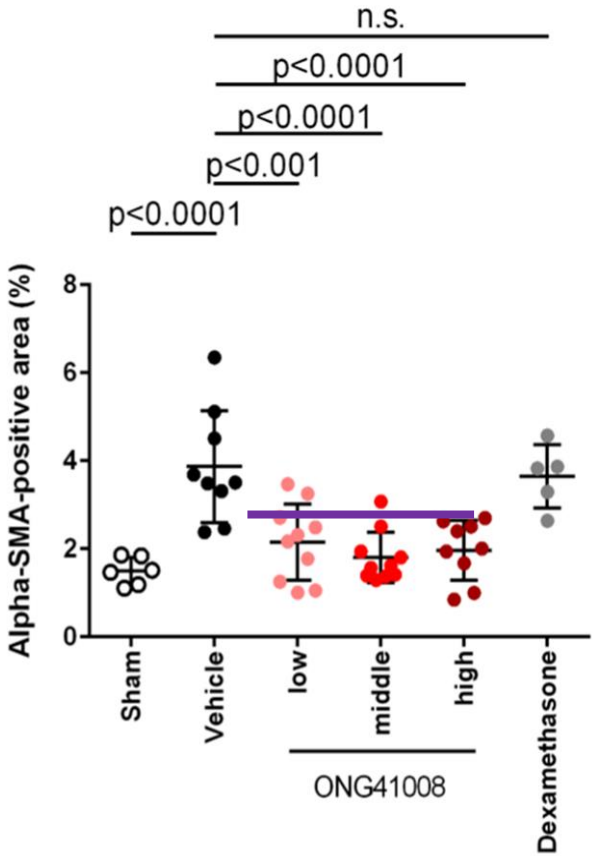

Low: ONG41008 10mpk
Middle: ONG41008 25mpk
High: ONG41008 50mpk
Dexamethasone 0.25mpk

Figure 6

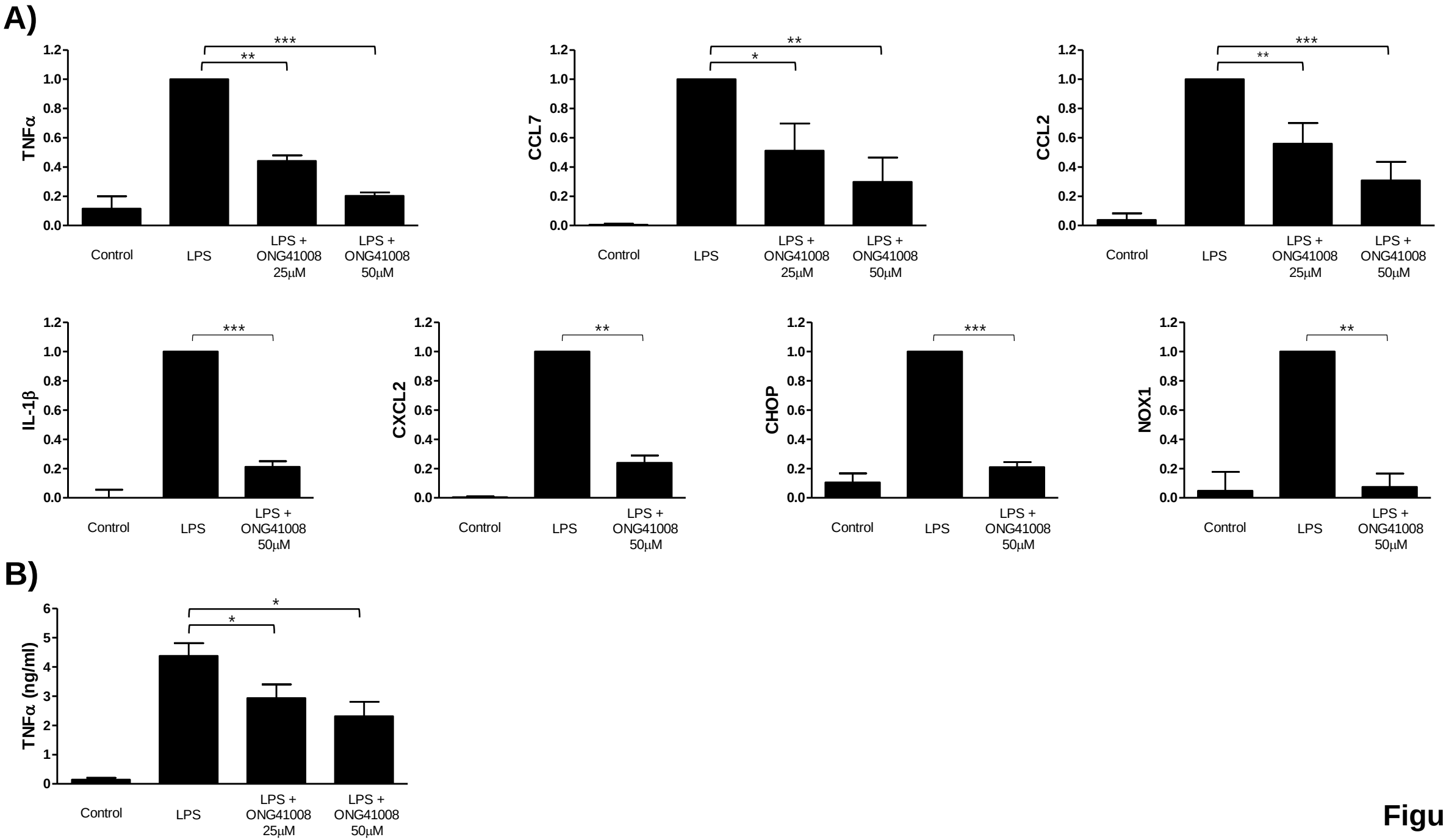
A)
TNFα
CCL7
CCL2
IL-1β
CXCL2
CHOP
NOX1
Control
LPS
LPS + ONG41008 25μM
LPS + ONG41008 50μM
B)
TNFα (ng/ml)

Figure 7

A)

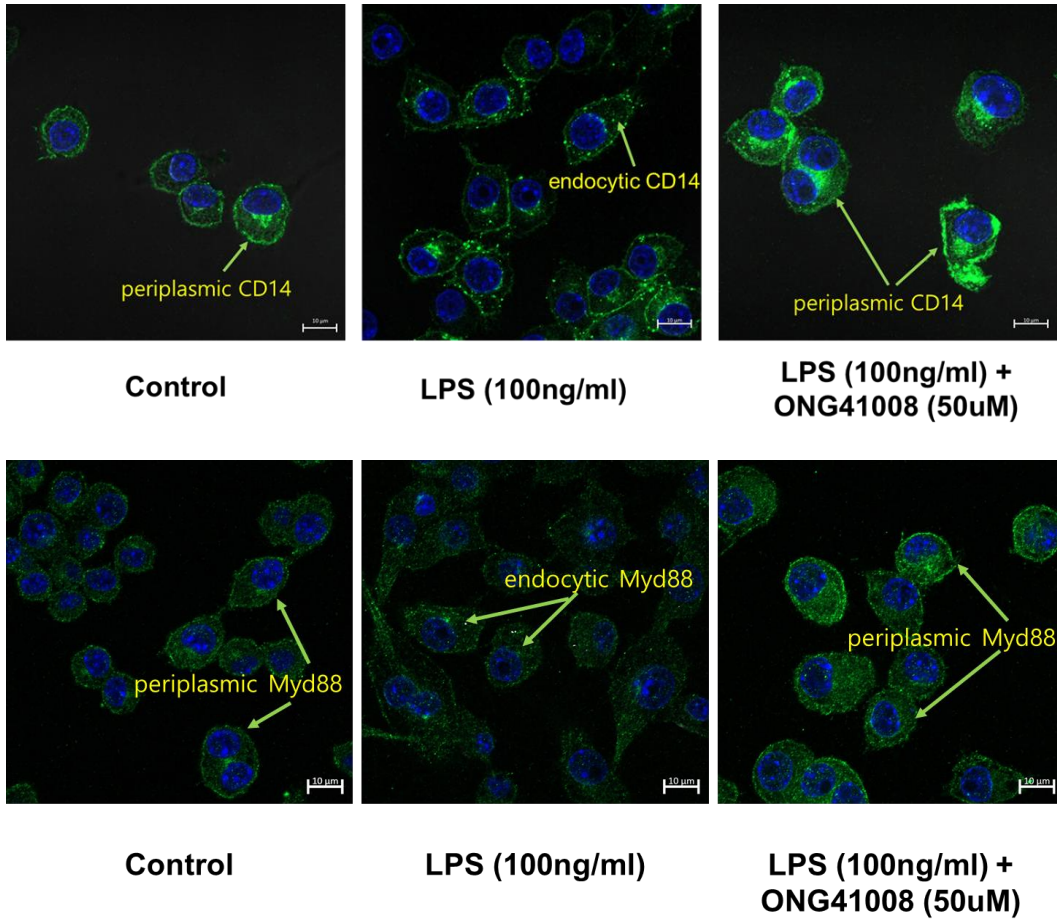
periplasmic CD14
endocytic CD14
periplasmic CD14
Control
LPS (100ng/ml)
LPS (100ng/ml) + ONG41008 (50uM)
periplasmic Myd88
endocytic Myd88
periplasmic Myd88
Control
LPS (100ng/ml)
LPS (100ng/ml) + ONG41008 (50uM)

B)

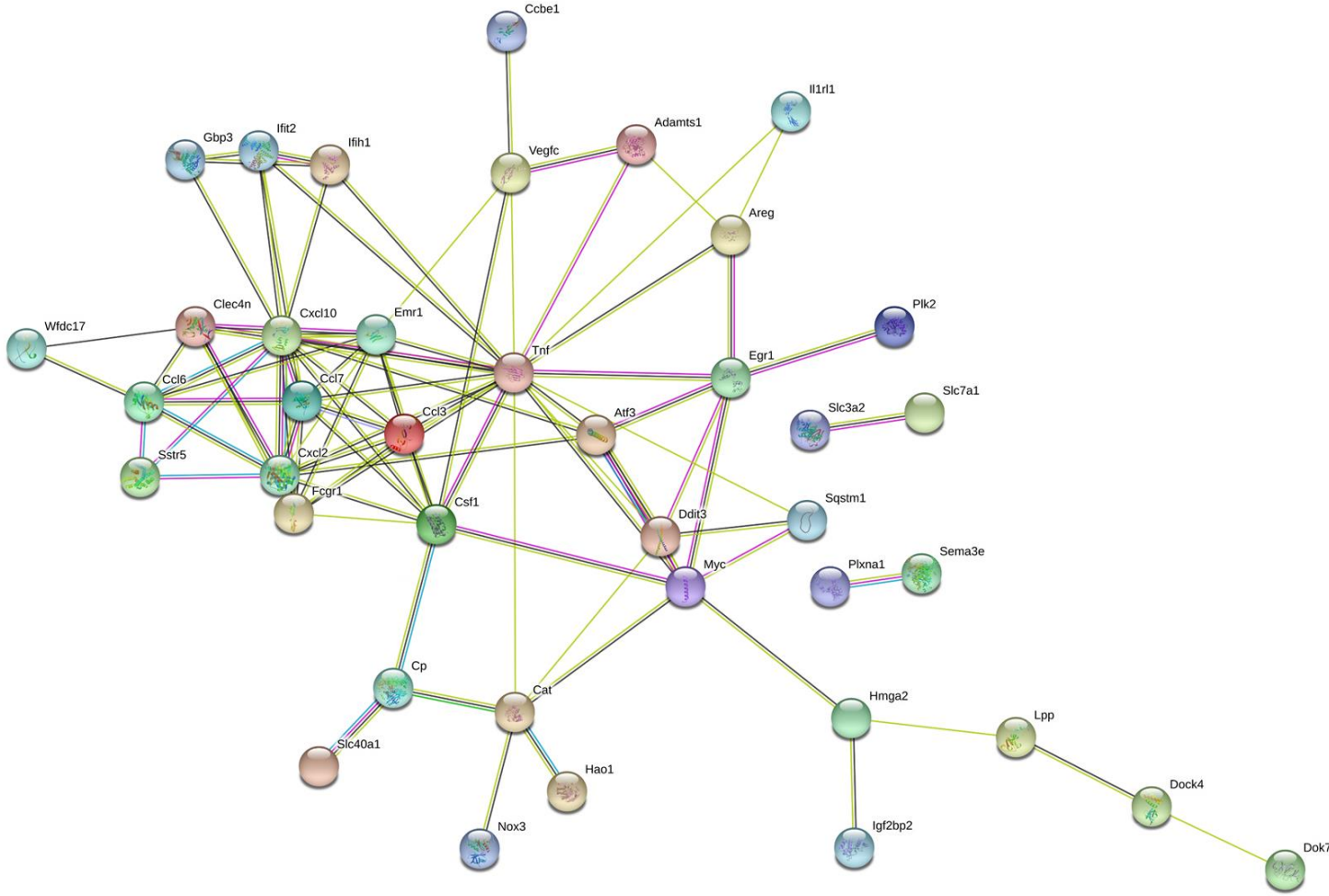
Ccbe1
Il1rl1
Adamts1
Gbp3
Ifit2
Ifih1
Vegfc
Areg
Wfdc17
Clec4n
Cxcl10
Emr1
Tnf
Plk2
Egr1
Ccl6
Ccl7
Ccl3
Atf3
Slc3a2
Slc7a1
Sstr5
Cxcl2
Fcgr1
Csf1
Ddit3
Sqstm1
Myc
Plxna1
Sema3e
Cp
Cat
Hmga2
Lpp
Slc40a1
Hao1
Dock4
Nox3
Igf2bp2
Dok7

Figure 8

A)

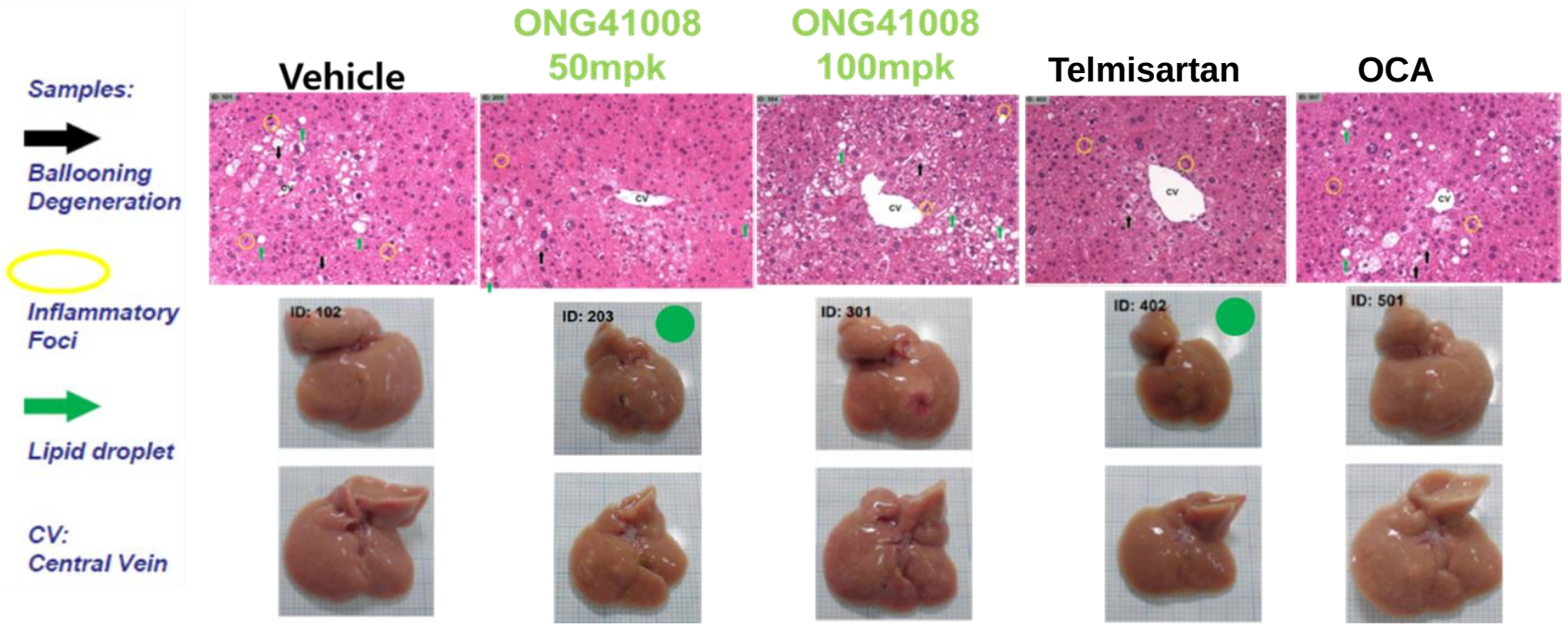

B)

Group	n	Score											NAS (mean ± SD)
		Steatosis				Lobular inflammation				Hepatocyte ballooning			
		0	1	2	3	0	1	2	3	0	1	2	
Vehicle	8	3	5	-	-	-	-	2	6	1	5	2	4.5 ± 0.8
Compound low	6	3	3	-	-	-	1	2	3	3	2	1	3.5 ± 0.8
Compound high	8	2	6	-	-	-	-	3	5	2	6	-	4.1 ± 0.6
Telmisartan	7	5	2	-	-	-	1	5	1	2	4	1	3.1 ± 1.2
OCA	8	3	5	-	-	-	-	6	2	2	4	2	3.9 ± 1.1

Definition of NAS Components

Item	Score	Extent
Steatosis	0	<5%
	1	5-33%
	2	>33-66%
	3	>66%
Lobular Inflammation	0	No foci
	1	<2 foci/200x
	2	2-4 foci/200x
	3	>4 foci/200x
Hepatocyte Ballooning	0	None
	1	Few balloon cells
	2	Many cells/prominent ballooning

C)

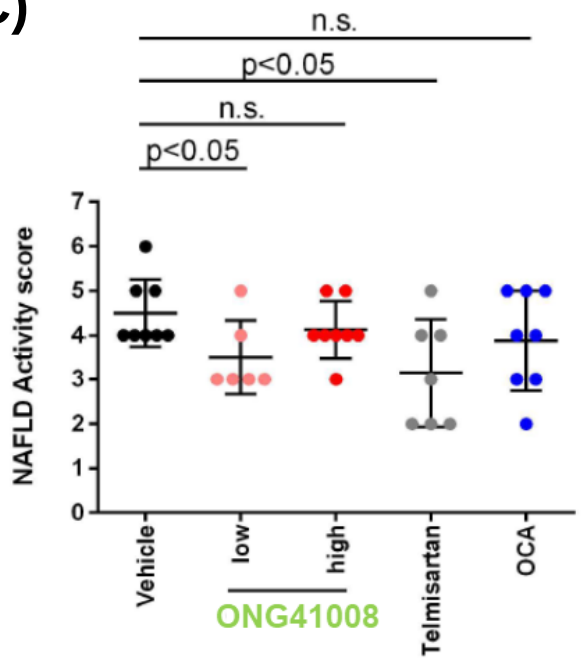

Figure 9